Final Report for Award G18AP00033

Project title:

Determination of near-surface shear velocity and Vs, Vp, and thickness of unconsolidated sediments using high-frequency teleseismic receiver functions across the U.S.

Principal Investigator:

Dr. Vera Schulte-Pelkum
Cooperative Institute for Research in Environmental Sciences (CIRES) and
Department of Geological Sciences
University of Colorado Boulder, UCB 399
Boulder, Colorado 80309
Telephone: (303) 919-0746
vera.schulte-pelkum@colorado.edu

Name of recipient:

University of Colorado Boulder
Office of Contracts and Grants
3100 Marine Street, ARC
572 UCB
Boulder, Colorado 80309-0572
P (303) 492-6221

Dates covered by this award:

June 1, 2018 – May 31, 2020

This material is based upon work supported by the U.S. Geological Survey under Grant No. G18AP00033.

Abstract

I analyzed receiver functions across the U.S. using data from the continent-wide EarthScope Transportable Array to extract information about the shallow subsurface. The arrival angle of teleseismic P body waves at the free surface is related to the near-surface shear velocity (V_s). Since shallow V_s is related to site amplification, it is of interest for ground motion estimates. Receiver functions calculated in the time domain show the radial to vertical component ratio at zero delay time, which is related to the free surface arrival angle. I calculated over a million receiver functions at 1832 stations and retained over 200,000 traces after quality control. This process was repeated using different frequency bands. Resulting apparent near-surface velocities show high geographical consistency and a strong correlation with physiographic and geological boundaries at the surface. Velocities especially in areas where basement is exposed at the surface are biased to higher values due to scattering effects in the receiver functions. Interestingly, neither apparent surface V_s nor the timing of a conversion from the shallow sediment-basement contact correlate to maps of either unconsolidated sedimentary thickness or depth to crystalline basement. However, it correlates closely to the horizontal to vertical particle motion ratio of ambient noise surface waves (Rayleigh waves). This suggests that the signal in receiver functions is a combination of near-surface velocities, layer thicknesses, and impedance structure. At shorter periods, theory derived using simple velocity models suggests that P incidence angles should sample shallower structure and therefore lower velocities. In the observations, some regions with high apparent V_s paradoxically show the opposite behavior, implying the need to employ more complex velocity models when calculating depth sensitivities.

When compared to the National Crustal Model (NCM) with values west of 100° longitude and provisional values east of 100° longitude, the estimated V_s shows strong similarity in patterns with NCM V_s near 100 m depth. However, the estimated V_s values are higher than those in the NCM. This suggests the estimated V_s samples depths near 100m and shallower, but is biased upward from true values in many cases. Observed behavior that runs counter to predictions using simple isotropic layer-over-halfspace models implies a strong dependence on complexity in more realistic near-surface velocity profiles. A modeling approach to scaling observed teleseismic and surface wave particle motion to site amplification may be a viable alternative to using velocity proxies such as Vs30.

Report

Introduction

Earthquake damage can be exacerbated at sites where soft soil and sedimentary basins lead to amplification of ground shaking. It is therefore important to characterize site response accurately in order to assess seismic hazard. Proxies in standard use are Vs30,

the averaged shear wave velocity to 30 m depth, and basin depth in shallow shear velocity models, where depth to the contours of V_s = 1.0 km/s (Z1.0) and 2.5 km/s (Z2.5) are used as proxies for basin depth. These values may be measured directly or estimated by using other proxies.

The availability of local seismicity and dense seismic networks in the tectonically active western U.S. drove the development of site amplification estimates and site response proxies in the past. While seismic hazard is also present in parts of the central and eastern U.S. (CEUS), past paucity of instrumentation and fewer local earthquakes have resulted in a lag for these areas in terms of site effect studies compared to the western U.S. Weak-motion sensor instrumentation in the central and eastern U.S. has recently increased significantly due to the passage of the EarthScope Transportable Array (TA), adoption of the CEUS network, and instrumentation of areas with recent induced seismicity. The nationwide coverage offers an opportunity to evaluate site responses in a uniform manner.

Continent-wide studies targeting deeper Earth structure show strong near-surface effects on weak-motion waveforms. Receiver functions are calculated by removing source and far-path signature (represented by the vertical component seismogram) from the radial component by deconvolution to obtain near-station structure. Multiple receiver function studies across the TA have found a strong imprint of a shallow layer with low shear velocity across large portions of the continent.

Estimation of near-surface V_s via the free surface effect on P

The approach used here to derive near-surface V_s from weak motion teleseismic data uses the fact that in a halfspace model, the particle motion angle of a P wave at the Earth's surface only depends on two parameters, the incident slowness p and the shear velocity V_s within the halfspace. An incident P wave with slowness p interacts with the free surface near the location of the seismometer. The free-surface P arrival angle i at the seismometer deviates from the incidence angle below the free surface, and can be measured from the arrival's component amplitude ratio:

$$\tan i = \frac{R}{Z} \tag{1}$$

Here, R is the radial (horizontal) component of the P arrival and Z the vertical component. The apparent shear velocity V_s^{app} below the free surface can then be calculated from this measured free surface angle i and the incident slowness p via the following:

$$V_s^{app} = \frac{1}{p} \sin \frac{i}{2} \tag{2}$$

This expression is derived in *Wiechert* (1907) *Nuttli and Whitmore* (1961) and used in e.g. *Ammon* (1991); *Svenningsen and Jacobsen* (2007); *Ni et al.* (2014); *Park and Ishii* (2018); *Park et al.* (2019).

Substituting equation 1, the apparent near-surface shear velocity is

$$V_s^{app} = \frac{1}{p} \sin(\frac{1}{2} \arctan \frac{R}{Z}). \tag{3}$$

For the radial and vertical free surface P amplitudes R and Z, *Svenningsen and Jacobsen* (2007) use the radial receiver function amplitude at zero delay time for R and calculate the autocorrelation of the vertical component for Z. However, in the iterative time deconvolution method for receiver function calculation used in this study (*Ligorria and Ammon*, 1999), receiver function amplitude is in itself an absolute horizontal to vertical ratio, in the case of the radial receiver function R/Z. In *Svenningsen and Jacobsen* (2007), the vertical autocorrelation used at zero delay is always 1. The radial receiver function amplitude at zero delay time is therefore used in the following to estimate V_s^{app}.

The relationship between R/Z and V_s^{app} is shown in Figure 1. Any amplification of the receiver function arrival not in the isotropic 1-dimensional model underlying the theory will lead to overestimation of V_s.

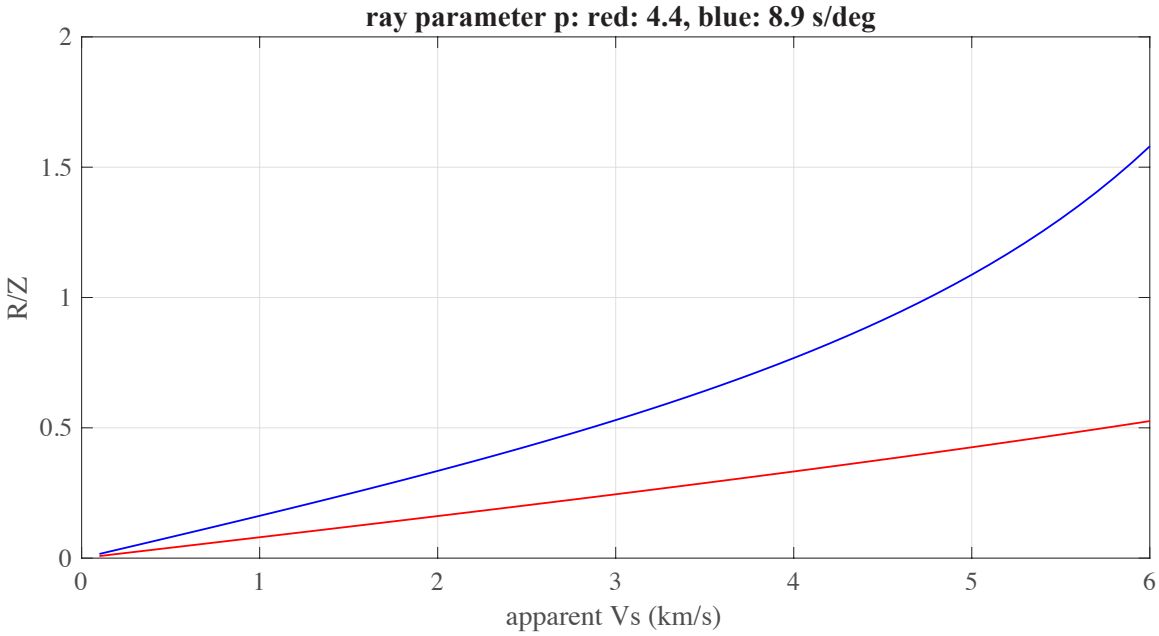

Figure 1: Relationship between estimated shear velocity and receiver function amplitude R/Z for approximate minimum and maximum ray parameters for teleseismic P.

Data

Receiver functions were processed for EarthScope stations across the continental U.S. Alaska was omitted from this initial analysis because of the lack of a USGS crustal model for comparison. All teleseismic events of magnitude 5.1 and greater at epicentral distances between 25° and 150° in 2-minute windows around the P or P_{diff} arrival predicted from a standard global velocity model. Radial component receiver functions were calculated using the time-domain iterative deconvolution method of *Ligorria and Ammon* (1999). Automated quality control was performed based on minimum signal-to-noise ratio, minimum variance reduction in the deconvolution, and pulse length and amplitudes to exclude poorly conditioned deconvolutions, with details as in the processing

described in *Schulte-Pelkum and Mahan* (2014). The data set was updated relative to that in *Schulte-Pelkum and Mahan* (2014) to reflect increased station coverage and data years by EarthScope stations. A total of 200,000 receiver functions at 1832 stations were retained from an initial >1 million receiver functions before quality control. The process was conducted twice using filter bands with a Gaussian factor of 3 (1 s pulse width) and 7 (0.5 s pulse width).

Results

V_s^{app} maps calculated from P initial arrival components using the zero-delay receiver function amplitude as in equation 3 are shown in Figure 2.

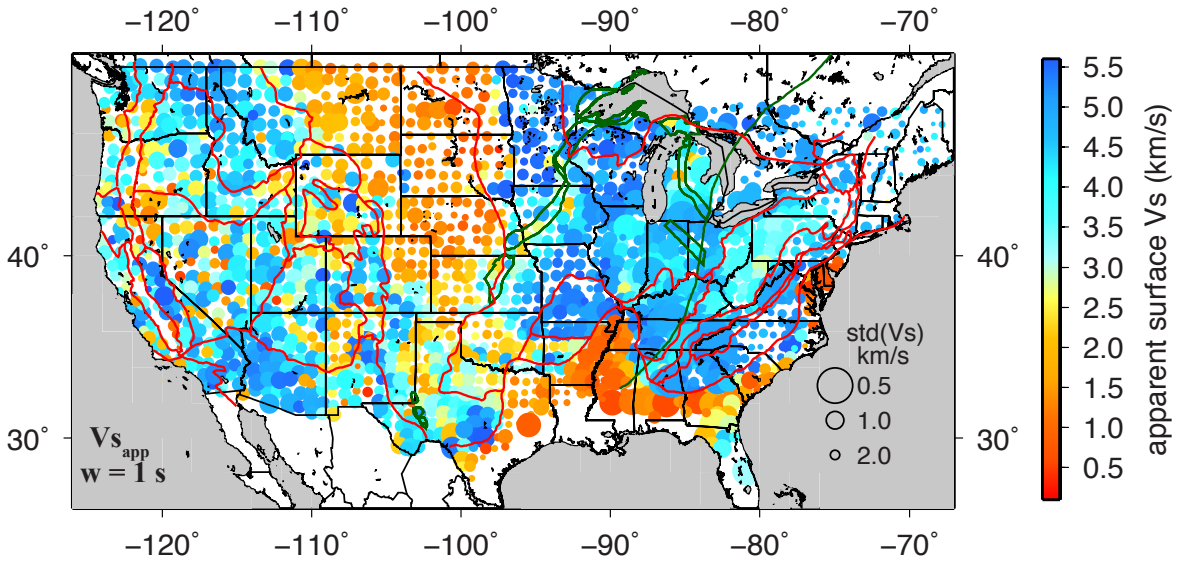

Figure 2: V_s^{app} calculated from receiver functions with pulse width 1 s. Red lines are physiographic province boundaries from *Fenneman and Johnson* (1946). Green lines are 1.1-1.0 Ga rifts and other volcanism and the Grenville front from *Whitmeyer and Karlstrom* (2007).

The results show high geographic coherence. Major areas with low surface velocity are the Denver, Powder River, and Williston basins but all with an eastward extension into glacial surface deposits, the Mississippi embayment, and Atlantic coastal plain. The Midcontinent rift appears as a low-velocity feature cutting otherwise fast areas. The Michigan and Appalachian basins show higher velocities than others such as the Permian, Ft. Worth, Anadarko, and St. Joaquin basins.

Areas with a speckled appearance can be correlated to geological features such as the Basin and Range province (where neighboring stations were placed on basement or intervening basin fill) and other small scale features such as the Black Hills in South Dakota, the Arkansas River Valley, and other small basins.

Many basement areas show apparent surface shear velocities exceeding 4.5 km/s. These are unlikely to be rock velocities, since shear velocities in crustal rocks are not ex-

pected exceed 4.1 km/s with the exception of mafic eclogite, an unlikely candidate (*Christensen*, 1996). The elevated values in V_s^{app} suggest bias from amplification of the zero-delay receiver function amplitude. This can occur from heterogeneity and near-surface anisotropy (*Schulte-Pelkum and Mahan*, 2014).

An example of high velocities is seen in the Ozark plateau. The surface geology is limestone and dolomite, which have high shear velocities that nevertheless are expected to be lower than the estimated velocities. The plateau's eastern edge merges into crystalline basement and shows a slight decrease in apparent Vs, albeit still above expected rock values. The Ouachita province to the south has surface exposures of sandstone and shales and shows lower apparent Vs. The E-W boundary between the two appears as a line with lower V_S^{app} in Figure 2. These stations are situated in the Arkansas river valley.

Figure 3 shows V_s^{app} estimated using higher frequency receiver functions, with a pulse width of 0.5 s. The higher frequency band leads to increased noise levels compared to the wider pulse receiver functions. As for the lower frequency case, the maps shows high geographical coherence. Among the differences to Figure 2 are a more pronounced decrease in velocity moving from the Williston/Powder River/Denver basins into glacial deposits in north Dakota to Nebraska and lower velocities over a larger area in the Michigan basin. A surprising difference is the apparent increase in velocities in most basement areas compared to the lower frequency case. This is counter to the expectation that lower frequencies sample deeper and usually higher velocities. From the geographical coherence, it appears that the estimated shear velocities are systematically related to surface geology, but the behavior based on the two frequency bands used does not appear to be a simple linear relationship to depth.

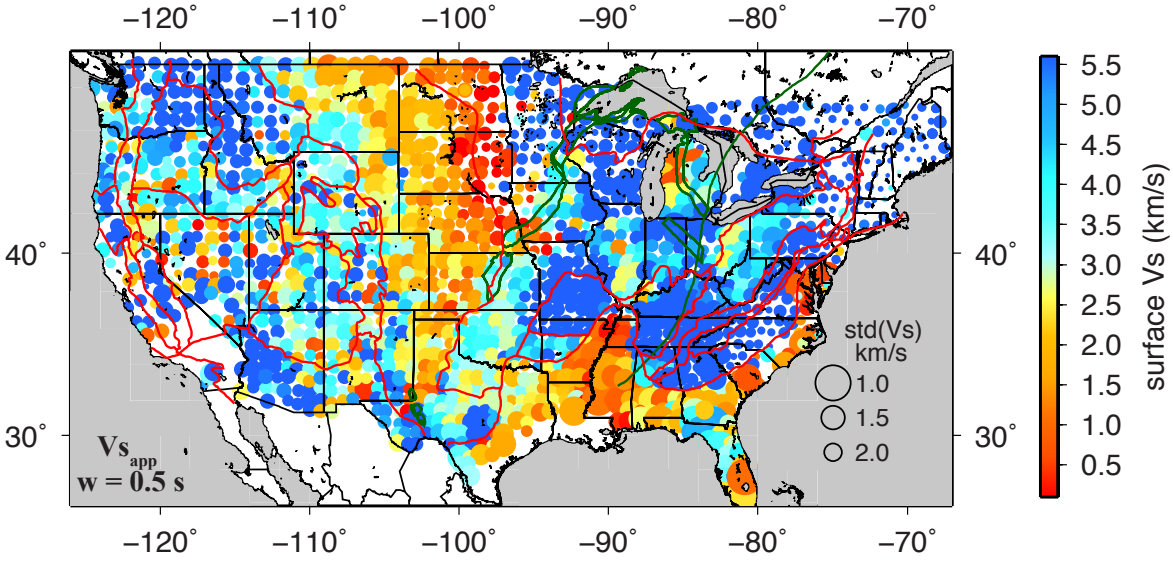

Figure 3: As in Figure 2, but calculated using receiver functions with pulse width 0.5 s.

Comparison to National Crustal Model, USGS NEHRP sites, and USGS Vs30 model

The character of V_S^{app} is explored further via comparisons to the USGS NCM, NEHRP Vs30 sites, and the USGS Vs30 model. Figure 4 shows shear velocity depth profiles from the NCM in comparison to V_S^{app} estimated using 1 s and 0.5 pulse width receiver functions. The first two locations with low estimated surface velocities show a lower V_S^{app} at higher frequencies, as one may expect from shorter wavelengths in the presence of a positive velocity gradient with depth. However, the other four sites show faster V_S^{app} at higher frequency, even where no velocity inversions are seen in the NCM profile. *Svenningsen and Jacobsen* (2007) and *Park et al.* (2019) conducted modeling to estimate the depth sensitivity of the P arrival angle for simple isotropic layer-over-halfspace cases and found a strong frequency dependence with sensitivity close to the surface, concentrated to a thickness much less than the wavelength. The results here suggest that for realistic velocity models, the behavior is even more complex. The polarization angle may be influenced by near-surface gradients and impedance contrasts in addition to 3-dimensional heterogeneity and near-surface anisotropy.

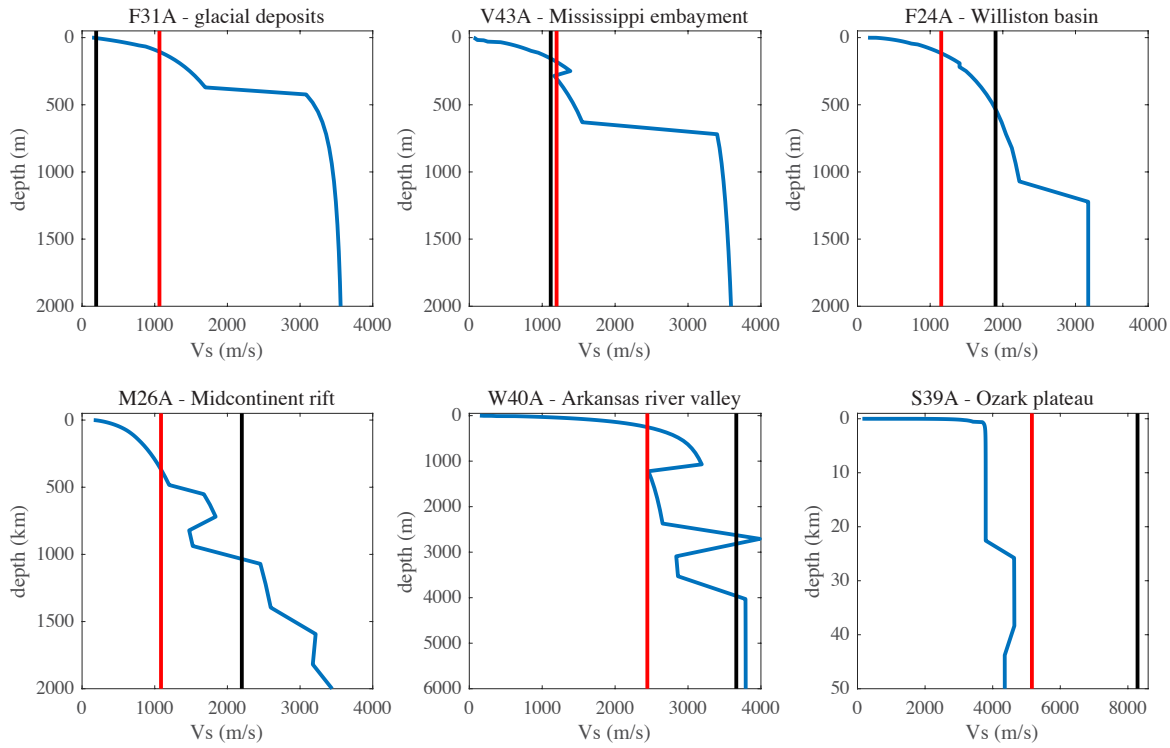

Figure 4: Shear velocity profiles as a function of depth for 6 representative locations. Blue line shows V_s from the NCM. Red vertical line is V_S^{app} estimated using receiver functions with pulse width 1 s, black vertical line using 0.5 s. Note changes in depth scale between locations.

The estimated shear velocities are compared to NCM shear velocities at a range of depths in Figure 5. While estimated shear velocities reach high values only reached deeper in the crust or in some cases not anywhere in the crust (e.g. S39A in Figure 4),

the observed geographical patterns show more similarity to shallower layers of the NCM than even layers at a few km depth. This is consistent with conclusions from previous modeling (*Park et al.*, 2019) that the sensitivity is shallow.

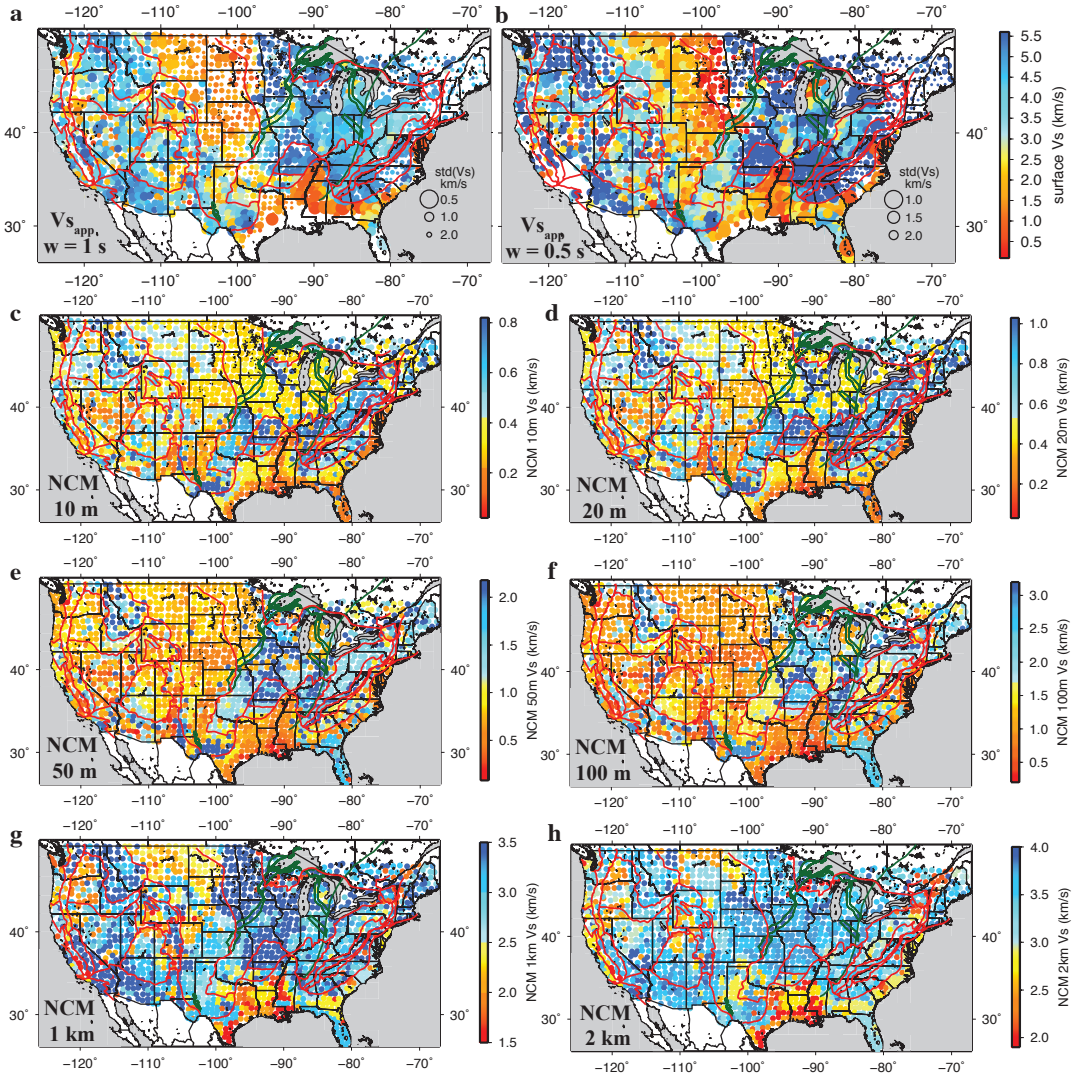

Figure 5: V_S^{app} and NCM depth slices for comparison. (a) V_S^{app} using pulse width 1 s (same color scale as b), (b) pulse width 0.5 s. (c - h) NCM shear velocity at indicated depths.

Estimated velocities show a gradient from slow to slower going from the Rocky Mountain Front in Montana and Wyoming to glacial deposits in eastern North and South Dakota. This trend is seen in NCM velocities at shallower depths, but not at 1 km depth and below (Figure 5, 6). The overall patterns of large areas with low V_S^{app} is similar to NCM depths to 100 m, decorrelates somewhat compared to NCM V_s at 1 km, and is dissimilar at 2-4 km. High V_S^{app} appears similar to NCM V_s to 1 km depth, but not deeper.

Considerations of wavelength (*Svenningsen and Jacobsen*, 2007; *Park et al.*, 2019) and observations (e.g., Figure 4) suggest different depth sensitivities between areas with surface basement and areas with low surface velocities. Figure 7 shows the two sets for V_S^{app} from

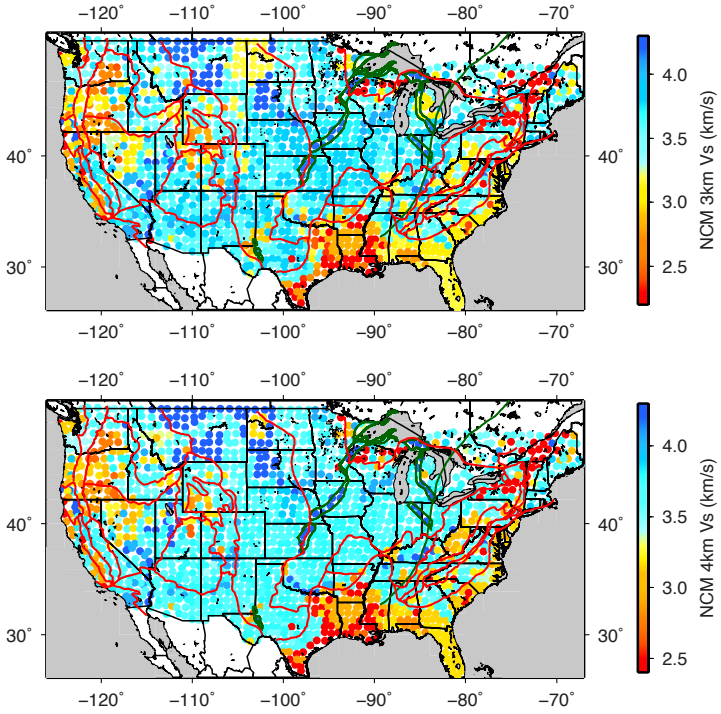

Figure 6: NCM deeper shear velocity slices for comparison. (top) 3 km, (bottom) 4 km depth.

1 s pulse width on separate maps, along with NEHRP Vs30 site types as well as the USGS Vs30 model from topographic proxy. The distribution of slow and fast areas has a high qualitative correlation with NEHRP sites and with the shallower NCM models shown in Figure 5. As in the comparison with NCM, the absolute velocities are higher in V_S^{app}, in many areas too high for shear velocities in crustal rocks. The correlation to the USGS Vs30 model (Figure 7f) is not very good, particularly for carbonate areas. This is not surprising because most of these areas have a Vs30 derived from topographic gradients as a proxy.

Implications for site amplification

The estimation of apparent near surface shear velocity from receiver function shows a strong influence of complexities of the velocity model. There will be no simple scaling from these results to velocity values at given depths. However, rather than taking this conclusion as a reason to dismiss teleseismic weak sensor response as an input for site amplification, it is worth considering that site amplification likely shows a similarly complex frequency-dependent relationship on shallow velocity structure. An alternative approach to relying on shallow shear velocity or Vs30 as a proxy may be to use horizontal amplification and refraction near the surface observed in ambient noise surface waves and teleseismic body waves and relate them directly to site amplification. Figure 8 shows maps of near-surface effects on receiver functions and surface waves. The upper map shows the delay in the peak initial arrival in receiver functions using 1 s pulse

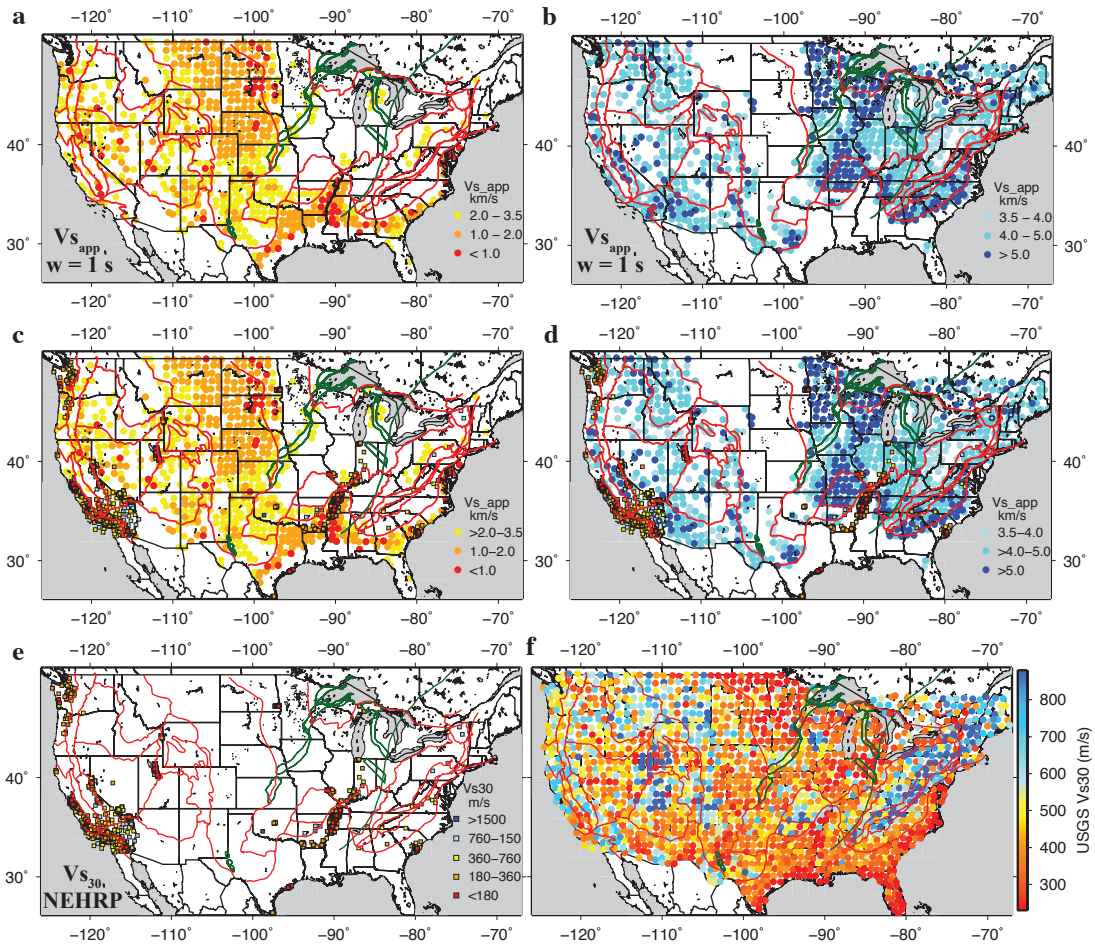

Figure 7: (a) High and (b) low values of V_S^{app} estimated using 1 s pulse width. (c) is the same as a, (d) same as b, except with NEHRP sites added (squares). (e) NEHRP sites only, with same color scale as in c and d. (e) USGS Vs30, in most areas from topographic proxy.

width. This quantity is closely related to the initial amplitude used to estimate V_S^{app}. In the absence of a near-surface low-velocity layer, the initial peak occurs at zero delay time. When a low-velocity surface layer is present, the initial peak is diminished in amplitude at zero time (Eqn. 3) and the initial peak shifts to later times and is dominated by the conversion at the bottom of the low-velocity layer (*Schulte-Pelkum et al.*, 2017). The peak delay in receiver functions shown in Figure 8 is therefore closely correlated to V_S^{app} (Figure 2). It also displays a startlingly close resemblance to Rayleigh wave H/V ratios derived from ambient noise (Figure 8), another observable that is strongly influenced by near-surface structure. Both measures as well as receiver function zero delay amplitude offer constraints on site amplification. Rather than scaling to velocity models, which is nonunique, a promising approach may be to perform forward modeling to predict these weak-acceleration responses to a range of realistic shear velocity profiles as provided by the NCM using forward modeling. The results could be related to ground shaking using forward modeling for the latter with the same realistic velocity profiles.

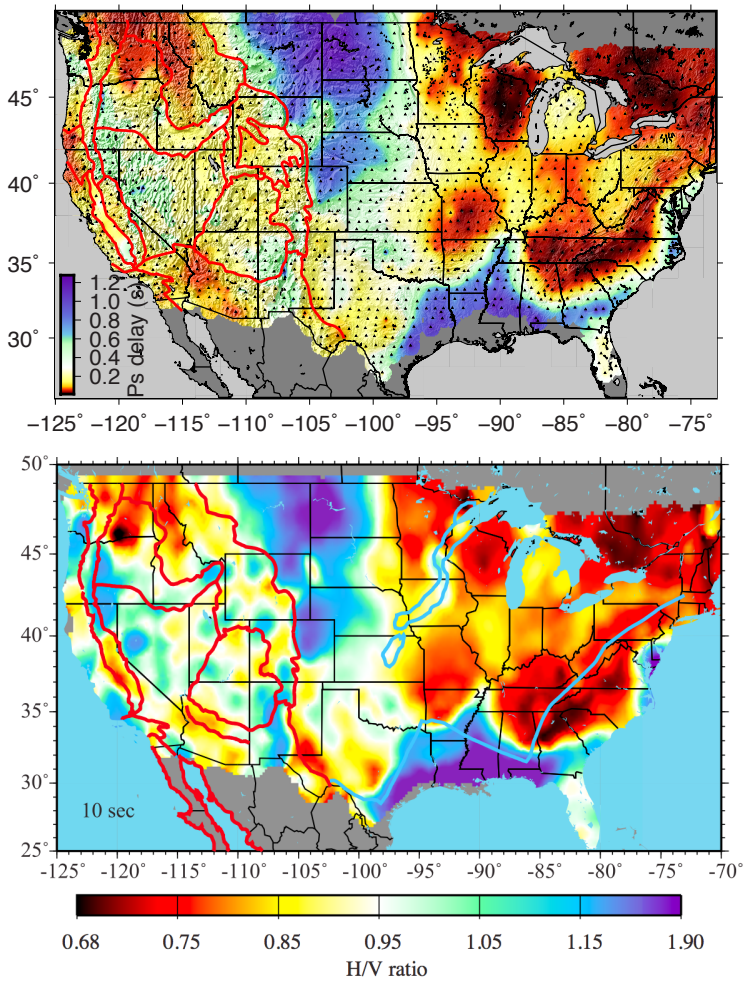

Figure 8: (top) Delay of initial peak in receiver functions with 1 s pulse width. (bottom) Horizontal to vertical component particle motion ratio of 10 s period Rayleigh waves from ambient noise (*Lin and Schmandt*, 2014).

Project data

No new seismic data were recorded as part of this work. All waveforms used are publicly available at the Incorporation Institutions for Research in Seismology's (IRIS) Data Management Center (DMC). Derived products (tables of station name, location, V_S^{app}) will be published as supplementary material in a peer-reviewed journal.

Bibliography

Presentations at professional meetings

- (Invited) Schulte-Pelkum, V. Ball, J., Sheehan, A.F., 2019-10-9: Analysis and removal of sediment signal in receiver functions. SAGE/GAGE annual workshop - SIG meeting, Portland, OR, US.
- Schulte-Pelkum, V. Ball, J., Becker, T., Porritt, R., Behr, W., 2019-9-8: Analysis and removal of sediment signal in receiver functions. Southern California Earthquake Center annual meeting, Palm Springs, CA, USA.

Peer-reviewed journal article

- Schulte-Pelkum, V., Estimation of near-surface shear velocity using teleseismic P arrival angles: Results for the EarthScope Transportable Array, in prep.

References Cited

Ammon, C., The isolation of receiver function effects from teleseismic P waveforms, *Bull. Seismol. Soc. Am.*, *81*, 2504–2510, 1991.

Christensen, N., Poisson's ratio and crustal seismology, *J. Geophys. Res.*, *101*(B2), 3139–3156, doi:10.1029/95JB03446, 1996.

Fenneman, N., and D. Johnson, Physical Divisions of the United States, *U.S. Geological Survey, Washington, D.C.*, 1946.

Ligorria, J., and C. Ammon, Iterative deconvolution and receiver-function estimation, *Bull. Seismol. Soc. Am.*, *89*(5), 1395–1400, 1999.

Lin, F.-C., and B. Schmandt, Upper crustal azimuthal anisotropy across the contiguous US determined by Rayleigh wave ellipticity, *Geophys. Res. Lett.*, *41*(23), 8301–8307, doi: 10.1002/2014GL062362, 2014.

Ni, S., Z. Li, and P. Somerville, Estimating Subsurface Shear Velocity with Radial to Vertical Ratio of Local P Waves, *85*(1), 82–90, doi:10.1785/0220130128, 2014.

Nuttli, O., and J. D. Whitmore, An observational determination of the variation of the angle of incidence of P waves with epicentral distance, *Bull. Seismol. Soc. Am.*, *51*, 269–276, 1961.

Park, S., and M. Ishii, Near-surface compressional and shear wave speeds constrained by body-wave polarization analysis, *Geophys. J. Int.*, *213*(3), 1559–1571, doi:10.1093/gji/ggy072, 2018.

Park, S., V. C. Tsai, and M. Ishii, Frequency-Dependent P Wave Polarization and Its Subwavelength Near-Surface Depth Sensitivity, *Geophys. Res. Lett.*, *46*(24), 14,377–14,384, doi:10.1029/2019GL084892, 2019.

Schulte-Pelkum, V., and K. H. Mahan, A method for mapping crustal deformation and anisotropy with receiver functions and first results from USArray, *Earth Planet. Sci. Lett.*, *402*(SI), 221–233, doi:10.1016/j.epsl.2014.01.050, 2014.

Schulte-Pelkum, V., K. H. Mahan, W. Shen, and J. C. Stachnik, The distribution and composition of high-velocity lower crust across the continental US: Comparison of seismic and xenolith data and implications for lithospheric dynamics and history, *Tectonics*, *36*(8), 1455–1496, doi:10.1002/2017TC004480, 2017.

Svenningsen, L., and B. H. Jacobsen, Absolute S-velocity estimation from receiver functions, *Geophys. J. Int.*, *170*(3), 1089–1094, doi:10.1111/j.1365-246X.2006.03505.x, 2007.

Whitmeyer, S. J., and K. E. Karlstrom, Tectonic model for the Proterozoic growth of North America, *Geosphere*, *3*(4), 220–259, doi:10.1130/GES00055.1, 2007.

Wiechert, E., Über Erdbebenwellen. Teil I: Theoretisches über die Ausbreitung der Erdbebenwellen, *Nachrichten von der Königlichen Gesellschaft der Wissenschaften zu Göttingen, Mathematisch - physikalische Klasse*, p. 415–529, 1907.